Korean J. Chem. Eng., 33(4), 1192-1199 (2016)
DOI: 10.1007/s11814-015-0254-0

pISSN: 0256-1115
eISSN: 1975-7220

Catalytic removal of CO and NOx using sol-gel synthesized $LaB_{0.5}Co_{0.5}O_3$ (B=Cr, Mn and Cu) and $LaMn_xCo_{1-x}O_3$ nano-perovskites

Behrang Izadkhah*,, Aligholi Niaei*,†, Daryush Salari**, Shahriar Hosseinpoor**, Seyed Ali Hosseini***, and Ali Tarjomannejad***

*Department of Chemical Engineering and Petroleum, University of Tabriz, Tabriz, Iran
**Department of Applied Chemistry and Chemical Engineering, University of Tabriz, Tabriz, Iran
***Department of Chemistry, Faculty of Science, Urmia University, 57159, Urmia, Iran
(*Received 10 February 2015 • accepted 26 November 2015*)

Abstract–Perovskite formulations of $LaB_{0.5}Co_{0.5}O_3$ (B=Cr, Mn and Cu) were examined and evaluated as catalyst for reduction of NOx by CO. Among the different and various formulations, $LaMn_{0.5}Co_{0.5}O_3$ showed the highest activity-selectivity with 89.84% conversion of NO and 9.62% yield of N_2O at 400 °C. Therefore, more precise evaluations were implemented on $LaMn_xCo_{1-x}O_3$ to find the optimum formulation. The $LaMn_{0.25}Co_{0.75}O_3$ included the maximum performance (68.79% conversion of NO at 350 °C and 92.85% at 400 °C) and N_2O yield (9.01); therefore, it was selected as optimum catalyst. Characterization methods were utilized to correlate activity and physical-chemical properties. The presented activity and reducibility of catalysts were improved due to partial substitution of Co^{3+} by B cation. Finally, no direct relationship was found between surface area and catalyst activity. The optimum catalyst showed complete activity-selectivity higher than 450 °C.

Keywords: Perovskite, $LaMn_xCo_{1-x}O_3$, NOx, CO, Catalytic Removal

INTRODUCTION

The emission of nitrogen oxides (NOx) is of great concern because of their important role in the environmental phenomena such as acid rain and photochemical smog formation [1]. Selective catalytic reduction (SCR), especially SCR using hydrocarbons (HC-SCR), is proven effective for NOx control [2-6]. Because CO was determined as an efficient reductant for NOx, the reaction between CO and NO is very important from a scientific point of view through the SCR process [7-10]. Utilizing the CO as the reductant for NOx has some advantages in practical application because of its significant presence in automobile exhaust. Moreover, CO has a poisonous nature because it can displace O_2 from the blood and can exacerbate heart problems, so there are strict government regulations for CO emissions. Simultaneous oxidation of CO to CO_2 and reduction of NO to N_2 helps industries to convert both of these poisonous gases into inert state without using any of the agents such as NH_3 which can lead to cost increase.

Similar to the other catalytic reactions, the type of catalyst plays the main role in the success of CO+NO reaction in certain conditions. It is necessary to know that the noble metal incorporated catalysts have the advantage of high activity at low temperatures for the mentioned reaction. However, they are expensive and the chance of deactivation by poisoning is high [11]. The perovskite-type mixed oxides attracted scientists' attention in the last decades as candidates for NO+CO reaction due to their redox properties and non-stoichiometric structure. The general chemical formula for perovskite compounds is ABO_3, where 'A' and 'B' are two cations of very different sizes, and O is an anion (often oxygen) that bonds to both; however, the 'A' atoms are larger than the 'B' atoms. Many metals are stable in the ABO_3 perovskite structure [12]. In addition, the perovskite compounds are able to tolerate significant partial substitution in A or B sites, which leads to oxygen excess or deficiency [13-15]. In the perovskite-type oxides, catalytic properties mainly depend on the nature of A and B ions and on their valence state. In fact, A atoms are in charge of structure stability of perovskite, and catalytic activity is generally determined by the B cation [16-19]. In addition to description, substitution at A site with ions, which includes the lower valence, can allow the formation of structural defects such as anionic or cationic vacancies and/or a change in the oxidation state of the transition metal cation to maintain the electro neutrality of the compound. Also, the B-site substitution of perovskites can be counted on as an effective way to improve their catalytic properties due to the generation of new lattice defects, mixed valence states and nonstoichiometric oxygen.

Among the various perovskite types with transition metal ions in B position, the mixed oxides, which contained Fe [20-23] and Cu [23-26] and their substitution with other transition metals, were evaluated for NO reduction by CO. He et al. [27] studied substitution of Mn with Cu and Ag for CO+NO reaction and concluded that Cu substitution was more effective than Ag substitution. Ciambelli et al. investigated the various metals in A site, which included La, Nd, Sm and partial substitution of Fe, by using Mn in CO oxidation. Note that the obtained sequence of A site metals for high activity in CO oxidation is La>Nd>Sm based on their studies [28]. Moreover, Cu was utilized for modifying the $LaCoO_3$ and the re-

†To whom correspondence should be addressed.
E-mail: niaei@yahoo.com, aniaei@tabrizu.ac.ir

sults of catalytic tests revealed that the activity of catalyst was increased significantly. Also, the creation of oxygen vacancies as a result of modification by Cu, which resulted in non-stoichiometric composition formation, was observed as the main reason for catalytic activity improvement by characterization tests including O_2 and NO_2 TPD [29]. Similar results for modifying the $LaCoO_3$ were achieved in the other catalytic process, which included volatile organic compound removal [30]. Therefore, oxygen vacancy creation during the modification of $LaCoO_3$ which leads to better adsorption and dissociation of reactants was the main reason for catalytic activity improvement [29]. The Co, Mn, Cu and Cr were determined and diagnosed as the transition metals which could be utilized as the catalyst active phase because of various valences that they could own [31]. In addition, it was proven that mentioned metals were able to be stabilized in the unconventional oxidation states in perovskite structure, which led to structural defects and high catalytic activity [32-34]. In the base of present researchers' findings and knowledge, there is no study about catalytic performance of partial substitution of Co in the perovskite formulation by using other transition metals including Mn, Cu, Cr and … for the removal of NOx.

This work aimed at establishing the relationship between the catalytic activity (NO conversion) and chemical-physical properties of $LaCoO_3$ and $LaB_{0.5}Co_{0.5}O_3$ (Cr, Mn, Cu) catalysts, which were obtained by sol gel combustion method. In addition, the evaluation of substitution value was carried out through the best catalyst to reach its optimum. Characterizing the catalysts by XRD, FTIR, BET, SEM, DLS and TPR techniques was the secondary aim of the present study, which was necessary to understand the relationship between the catalytic activity and chemical-physical properties.

EXPERIMENTAL

1. Catalyst Preparation

$La(NO_3)_3{\cdot}6H_2O$, $Co(NO_3)_2{\cdot}6H_2O$, $Cu(NO_3)_2{\cdot}3H_2O$, $Mn(NO_3)_2{\cdot}4H_2O$, $Cr(NO_3)_3{\cdot}9H_2O$ and citric acid monohydrate were the starting materials. $LaB_{0.5}Co_{0.5}O_3$ (B=Cr, Mn, Cu) catalysts were prepared by sol gel combustion method as described through the present researchers' earlier work [30]. Briefly, to ensure the complete complexation of the cations, citric acid was added over the stoichiometric amount to an aqueous solution of La, Co and B nitrates with cation ratios La : M : Co, of 1 : 0.5 : 0.5. The ratio of citric acid to nitrates was kept at 0.4. $LaMn_xCo_{1-x}O_3$ (x=0.1, 0.25) was synthesized by the sol gel method by applying the stoichiometric amount of manganese and cobalt nitrates.

The solution was left to evaporate the extra water at 80 °C with continuous mechanical stirring until a sticky gel was obtained. To carry out the gel decomposition under controlled conditions, the temperature was gradually raised to 200 °C and finally the decomposed gel self-ignited. The spontaneous combustion lasted for 10-20 s and gave rise to the powdered product. The combusted powders were then fired in static air at 700 °C for 6 h.

2. Catalyst Characterization

For FTIR spectroscopy, the samples were pressed into self-supporting wafers of 10-15 mg/cm^2 surface density and placed into a glass cell sealed by KBr windows. The spectra were recorded in transmittance at room temperature using a Bruker spectrometer (model TENSOR 27, USA).

Crystalline phases were identified by X-ray diffraction on a Siemens D500 diffractometer (Germany) and Cu K_α radiation (λ= 1.54 A). Diffractograms were recorded with a step of 4° per minute for 2θ between 15 and 75°. ICSD files were utilized as the patterns for phase recognition of resulting diffractograms, while the mean size of crystallites (D) was evaluated by means of the Scherrer equation, $D=K\lambda/(\beta\cos\theta)$, where K is a constant equal to 0.89, λ is the wavelength of the X-ray and β is the effective line width of the X-ray reflexion.

N_2 isotherms were measured at −196 °C by using a micro pore analyzer (ASAP 2010, USA) for determining the BET surface area and pore volume of samples.

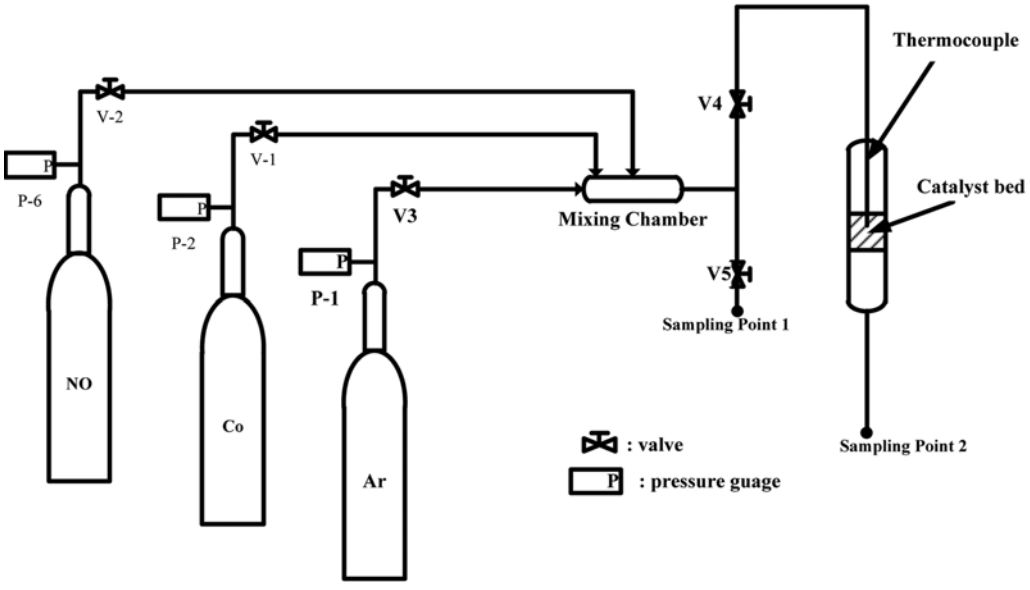

Fig. 1. Simple scheme of catalytic test set up for CO+NO reaction.

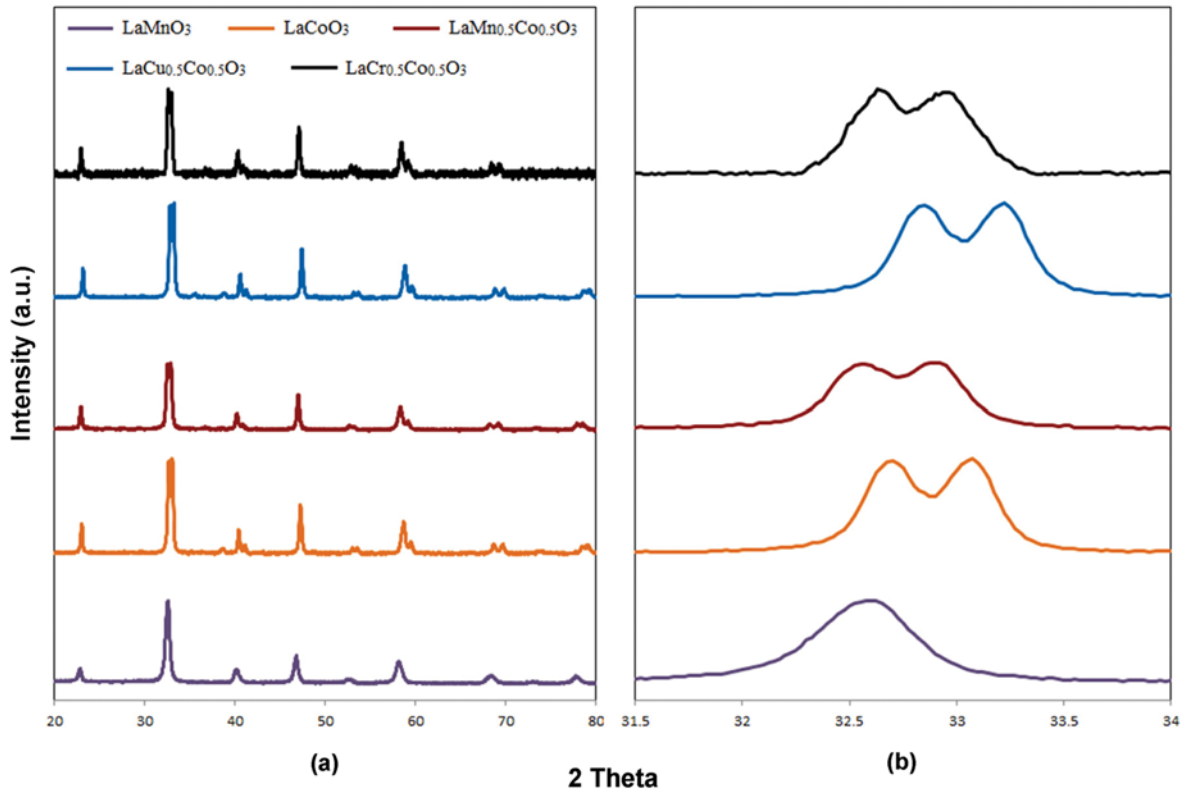

Fig. 2. X-ray patterns of $LaB_{0.5}Co_{0.5}O_3$ (B=Cr, Mn, Cu).

Temperature programmed reduction (TPR) measurements were carried out with Micromeritics Autochem 2900 (USA). Samples were pre-treated with a gaseous mixture containing 5 vol% oxygen in helium at 500 °C for 2 h. Hydrogen consumption was measured with a mixture of 5 vol% H_2 in argon at 20 cm^3min^{-1} and a linear heating rate of 10 °C/min at 50-950 °C.

The morphology of the mixed oxides was determined by scanning electron microscopy (SEM) by Tescan (Czech Republic) instrument with pre-coating samples with gold.

Particle size of samples was determined by dynamic laser light scattering (DLS) by Shimadzu SALD 2101 (Japan).

3. Catalytic Studies

A simple scheme of test setup can be seen in Fig. 1. The reaction of $CO+NO_x$ was carried out in a straight quartz reactor (l=60 cm (2 cm as catalyst bed), i.d.=0.8 cm) at different temperatures under atmospheric pressure. The catalyst (200 mg) was inserted between two quartz wool plugs. The temperature was controlled with K-type thermocouple. Before reaction tests, the catalysts were pretreated with air (40 cm^3min^{-1}) at 300 °C for 2 h. Total flow rate of feed was 200 cm^3min^{-1}. Feed composed of 3,000 ppm NO and 3,000 ppm CO was balanced with Ar. According to the above-mentioned arrangement, the gas hourly space velocity (GHSV) was fixed at about 12,000 h^{-1}.

The feed and product gases were analyzed with a Shimadzu 2010 gas chromatograph (GC) equipped with a TCD detector and a HP-MoleSieve (Agilent, USA)column (l=30 m, i.d.=0.53 mm) with helium as carrier gas. The samples of reaction products were injected by using a 1,000 μL Hamilton syringe.

RESULTS AND DISCUSSION

Through the synthesis routine, which can be termed as citrate method, the ratio of fuel to oxidant was kept at 0.4 as recommended by Deganello et al. [35]. They indicated that lower fuel to oxidant ratios avoid the segregation of dopant and provide small particle size. Also, the mole ratio of B/Co was adjusted on one because this value was the most common and the maximum possible substitution for substituted lanthanum cobaltites, as well as the high activity of 50% substitution lanthanum manganite has been reported in combustion of CO, previously [16].

The XRD patterns of synthesized catalysts can be seen in Fig. 2(a). Also, in Fig. 2(b), it is possible to see the accurate angle of most intensive peak of under study patterns. As it is possible to see in Fig. 2(b), all of $LaB_{0.5}Co_{0.5}O_3$ catalysts show different patterns compared to $LaCoO_3$. Main peaks for all $LaB_{0.5}Co_{0.5}O_3$ catalysts in comparison to $LaCoO_3$ were shifted due to 50 mol% metal doping. $LaCoO_3$ showed a pure rhombohedral structure (ICSD#156452), whereas $LaCu_{0.5}Co_{0.5}O_3$ showed a monoclinic crystal system. The relative intensity of the samples was different to some extent. Besides,

Table 1. BET surface area of perovskites

Perovskite	BET (m^2/g)
$LaCoO_3$	15
$LaCu_{0.5}Co_{0.5}O_3$	13.6
$LaCr_{0.5}Co_{0.5}O_3$	11.3
$LaMn_{0.5}Co_{0.5}O_3$	12.6

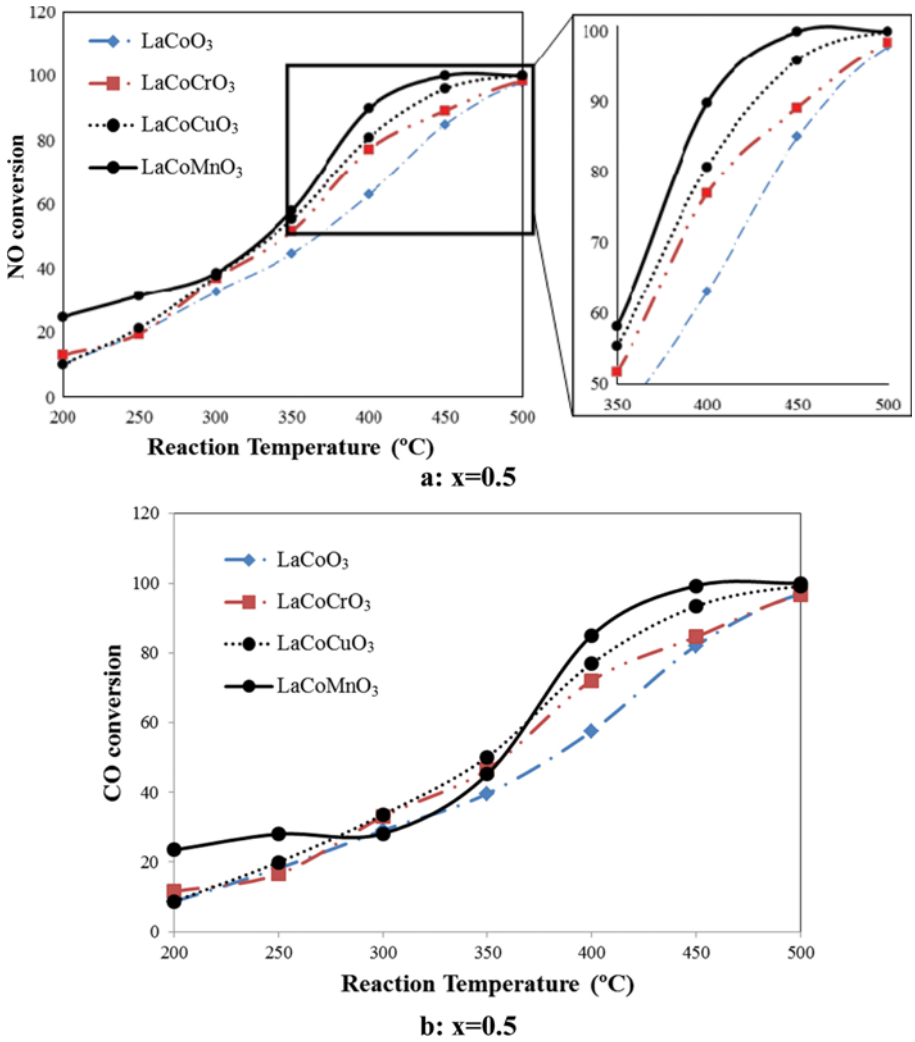

Fig. 3. (a) NO conversion versus reaction temperature for $LaCoO_3$ and $LaB_{0.5}Co_{0.5}O_3$, (b) CO conversion versus reaction temperature for $LaCoO_3$ and $LaB_{0.5}Co_{0.5}O_3$.

a little segregation of BO_x in $LaB_{0.5}Co_{0.5}O_3$ (≤5%) is possible.

BET method was utilized to determine the specific surface area of catalysts and results presented in Table 1. As can be seen, with substitution of Co by B metals the specific surface area of catalysts decreased. Cr and Cu substituted catalysts showed maximum and minimum decrease of specific surface area in comparison to $LaCoO_3$, respectively.

The synthesized perovskites were tested as the catalyst for NO+CO reaction for evaluating the effect of Co partial substitution on the catalytic activity. Conversion versus reaction temperature curves for $LaCoO_3$ and $LaCo_{0.5}B_{0.5}O_3$ are presented in Fig. 3. Through the present figure, for better understanding the differences in conversions for various formulations of synthesized perovskites, critical area of plot was managed into the other subset of related plot with more precision. That is, we focused on this area because various formulations showed their differences as more recognizable in the condition governing related area. For example, the difference between maximum and minimum conversion at 400 °C was about twice that at 350 °C (27.1 and 13.3, respectively).

Based on the results presented in Fig. 3, substitution of Co by Mn improved the activity of perovskite for NO+CO reaction. The sequence for the activity of various formulations in CO+NO reaction is as follows:

$$LaCo_{0.5}Mn_{0.5}O_3 > LaCo_{0.5}Cu_{0.5}O_3 > LaCo_{0.5}Cr_{0.5}O_3 > LaCo_0O_3.$$

Another important feature of a catalyst through the NO+CO reaction is selectivity in N_2. For the reaction of CO+NO, two products can be achieved including N_2O and N_2. In fact, N_2O is an intermediate product considering following three step simple reaction mechanism [36].

$$2CO+2NO \rightarrow N_2+2CO_2 \quad (1)$$

$$CO+2NO \rightarrow N_2O+CO_2 \quad (2)$$

$$CO+N_2O \rightarrow N_2+CO_2 \quad (3)$$

For this reaction, the selectivity was defined by mole% of NO, which converted into N_2, as an inert product, by reaction with CO. Explained simply, there are two main products including N_2 and N_2O, and selectivity for each one can be calculated by mole%

of NO which converted to each one. Also, it was well known that for any reaction it is possible to calculate yield of each product by multiplying its selectivity to reaction conversion. Fig. 4 shows the yield of synthesized catalysts in N_2O at various temperatures

From Fig. 4, $LaCo_{0.5}Mn_{0.5}O_3$ has high yield of N_2O in lower temperatures in comparison to other catalysts. By increasing of reaction temperature, the yield of N_2O becomes lower and reaches 0 at 500 °C. This can be explained by completing of reaction in step 3 of the primarily mentioned mechanism. So, after 500 °C, all of reacted NO converted into N_2 which is an inert gas and can be counted as our goal for reaction.

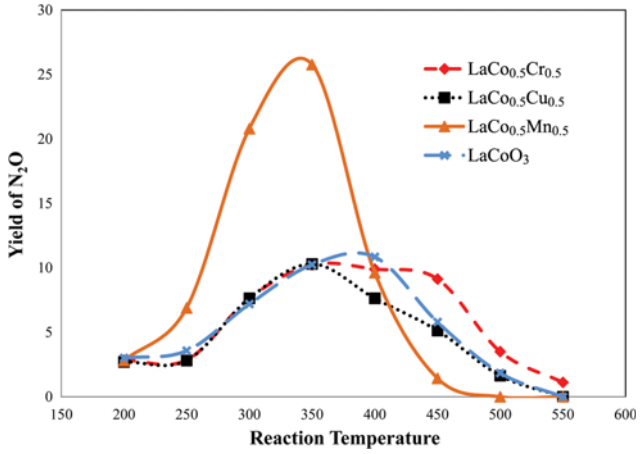

Fig. 4. Selectivity of synthesized catalysts in N_2O at various reaction temperatures.

The reducibility of the catalysts was studied by TPR analysis and the reduction profiles can be seen in Fig. 5.

The reduction of La_2O_3 occurs above 700 °C. The TPR profile of $LaCoO_3$ shows some separate peaks, which indicates the consecutive reduction of Co^{3+} to Co^{2+} ($LaCoO_{2.5}$) and $LaCoO_{2.5}$ to Co^0 at ranges 330-475 and 550-650 °C, respectively. In the case of TPR profiles of $LaB_{0.5}Co_{0.5}O_3$, the reduction temperature of cobalt decreased, in comparison to reduction temperature of Co^{3+} in $LaCoO_3$, which revealed that introduction of Cu, Cr, and Mn promoted the reduction of cobalt in the perovskites. In the case of $LaMn_{0.5}Co_{0.5}O_3$, the first peak of the TPR profile around 400 °C is due to the removal of oxygen from perovskite. In the TPR profile of $LaCu_{0.5}Co_{0.5}O_3$, the peak around 280 °C was ascribed to the reduction of Cu^{2+}. For $LaCr_{0.5}Co_{0.5}O_3$, a small peak was observed around 400 °C. It has been reported that Cr^{3+} in $LaCrO_3$ structure is highly stable, so it could not be reduced under the employed conditions through the present work. The peaks in present range of temperature were attributed to reduction of Co^{3+} and also to some La_2CrO_6 which could be formed during the synthesis of perovskite [30].

In the catalytic oxidation reactions, reducibility of catalyst is a prominent factor in the activity, whereas in oxidation/reduction reactions like CO+NO reaction, it could not be a prominent fac-

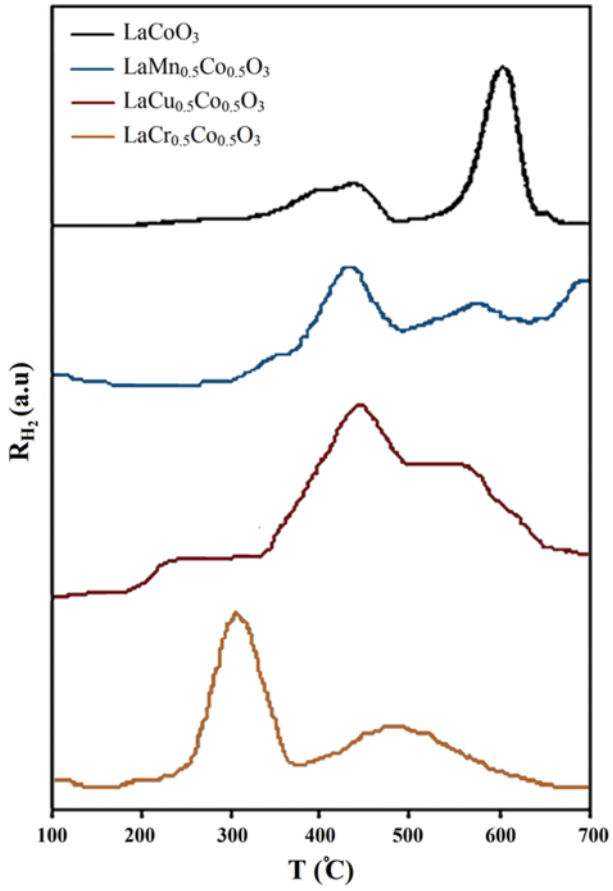

Fig. 5. TPR curves of $LaCoO_3$ and $LaMn_{0.5}Co_{0.5}O_3$, $LaCu_{0.5}Co_{0.5}O_3$, $LaCr_{0.5}Co_{0.5}O_3$.

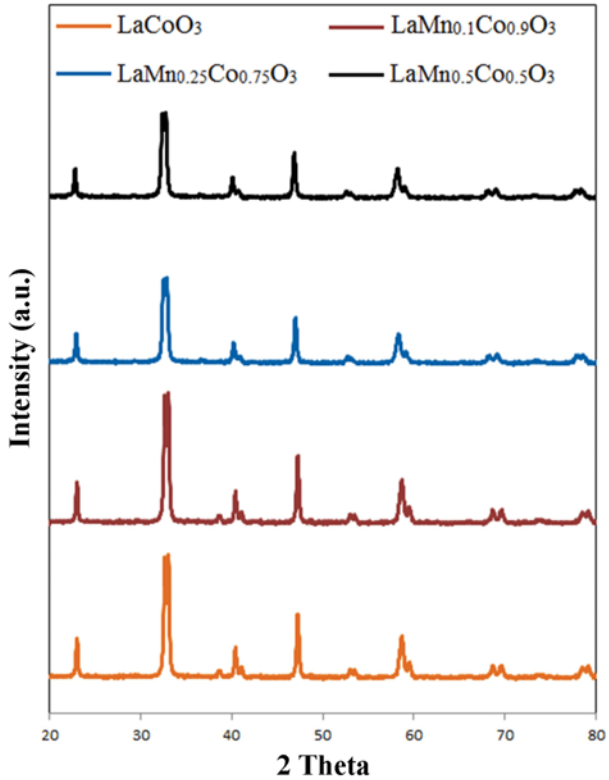

Fig. 6. X-ray patterns of $LaMn_xCo_{1-x}O_3$; (a) x=0, (b) x=0.1, (c) x=0.25, (d) x=0.5.

tor on activity and a catalyst with moderate oxidation/reduction property is more desired. $LaMn_{0.5}Co_{0.5}O_3$ showed higher catalytic activity despite having the lower reducibility in comparison to others. This is a logical conclusion because CO+NO reaction is an oxidation/reduction reaction, and a catalyst with only good oxidation or reduction property is not suitable for this reaction.

To find the best ratio of Mn to Co, $LaMn_xCo_{1-x}O_3$ (x=0, 0.1, 0.25, 0.5) catalysts were synthesized and studied. XRD patterns of $LaCoO_3$ and $LaMn_xCo_{1-x}O_3$ (x=0.1, 0.25, 0.5) can be seen in Fig. 6.

All characteristic peaks of perovskite phases were recognized at all patterns. The perovskites crystallized in a rhombohedral structure. The main differences of patterns were the shift of peak places and the intensity of peaks. A little shift to lower 2θ is observed for doped perovskites, which is due to a change in the d-spacing [18]. The intensity of peaks of $LaMn_xCo_{1-x}O_3$ is sharper than that of $LaCoO_3$, meaning the existence of larger crystallites in $LaMn_xCo_{1-x}O_3$.

The structure of $LaMn_xCo_{1-x}O_3$ (x=0.1, 0.25, 0.5) was studied by FTIR (Fig. 7). The broad band at 3,448 cm^{-1} was attributed to the presence of co-ordinate/entrapped water, which is rapidly adsorbed by KBr [18]. The bands around 540 and 450 cm^{-1} were at-

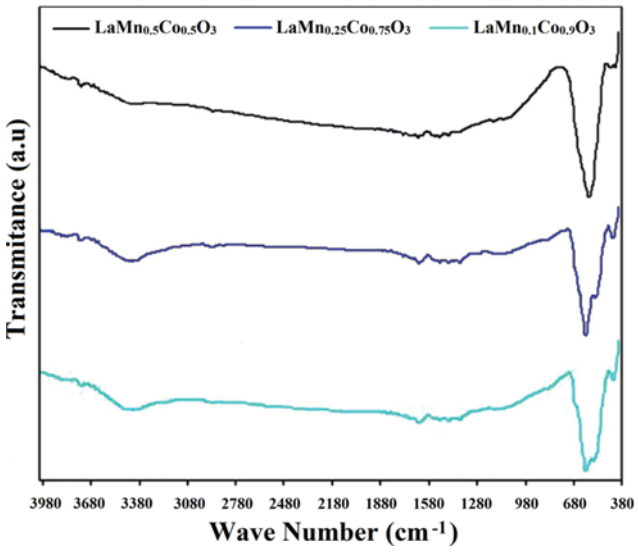

Fig. 7. FTIR spectra of $LaMn_xCo_{1-x}O_3$ (x=0.1, 0.25, 0.5).

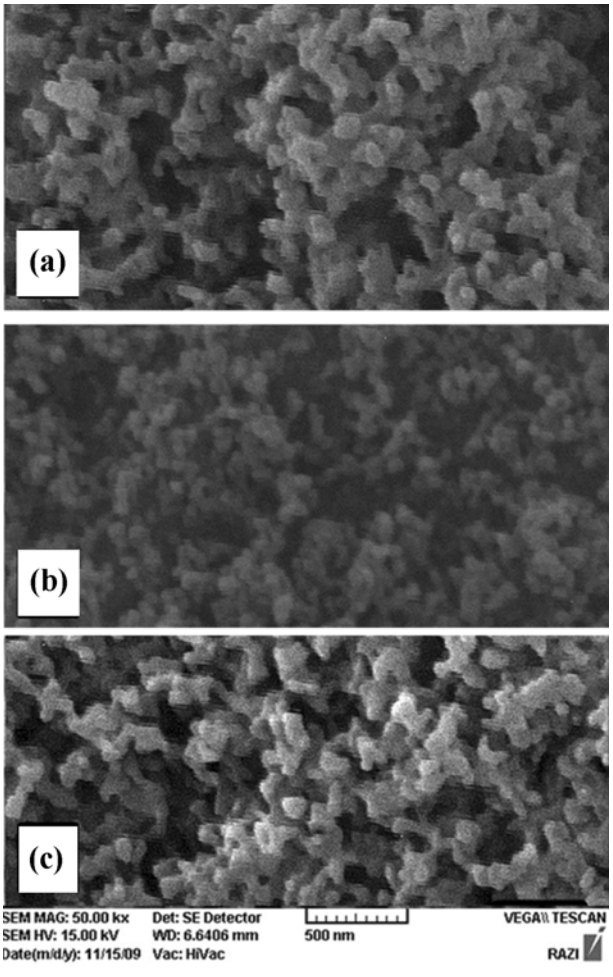

Fig. 8. SEM micrographs of $LaMn_xCo_{1-x}O_3$: $LaCoO_3$ (a), $LaMn_{0.25}Co_{0.75}O_3$ (b), $La\ Mn_{0.5}Co_{0.5}O_3$ (c).

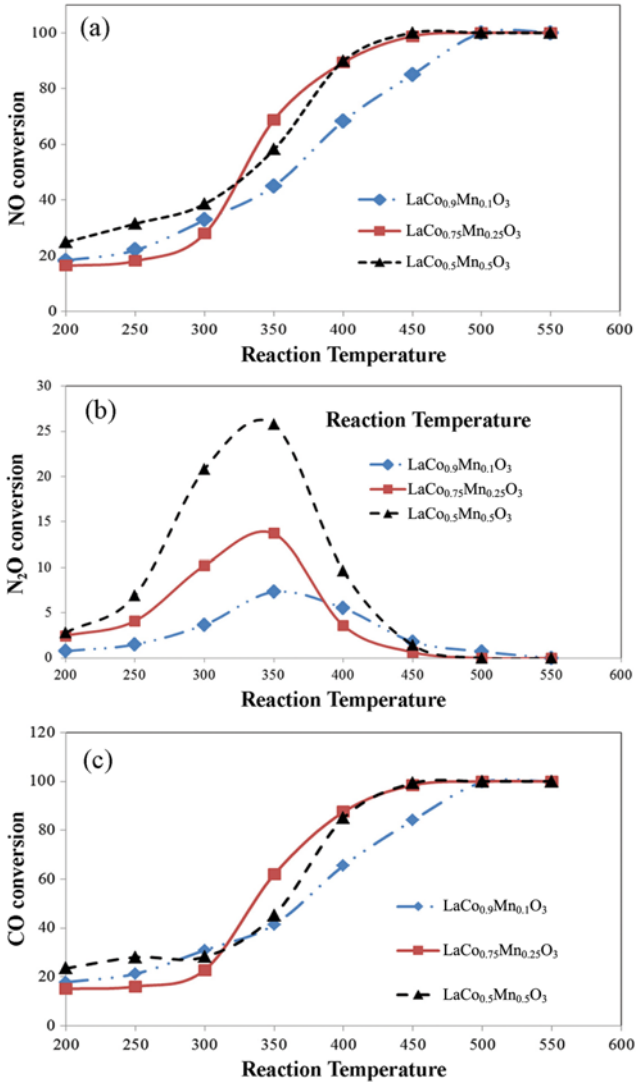

Fig. 9. NO conversion (a), N_2O yield (b) and CO yield (c) of $LaMn_xCo_{1-x}O_3$ (x=0.1, 0.25 and 0.5) perovskites in CO+NOx reaction.

Table 2. Particle diameter of the perovskites obtained by DLS

Particle diameter (nm)	Percentage of catalyst with mentioned mean particle diameter		
	$LaCoO_3$	$LaMn_{0.25}Co_{0.75}O_3$	$LaMn_{0.5}Co_{0.5}O_3$
241	0	0	1.214
196	0	0	1.951
159	0	5.714	4.731
129	0	20.070	18.127
105	3.128	28.535	25.535
85	28.423	30.205	26.205
69	32.634	15.463	11.463
56	21.752	0	10.644
46	12.327	0	0
37	1.731	0	0

tributed to the Co-O stretching vibration (ν_1 mode) and the O-Co-O deformation vibration (ν_2 mode), respectively. It was observed that the intensity of the band at 540 cm^{-1} decreased with an increase in cobalt substitution by manganese. The band seems to be two overlapped bands, ascribed to the appearance of manganese oxide with an increase in manganese loading.

The morphology and particle size of $LaMn_xCo_{1-x}O_3$ perovskites were studied by scanning electron microscopy. Fig. 8 shows the SEM images of perovskites.

All samples showed the porous features due to release of the large amount of gases during combustion. $LaCoO_3$ (Fig. 8(a)) exhibited rather spherical shape with mean particle size under 100 nm. The SEM micrograph of $LaMn_{0.25}Co_{0.75}O_3$ is shown in Fig. 9(b). As it is illustrated by SEM micrographs, agglomerates appeared to be thin waffles whose surfaces were perforated. The micrograph of $LaMn_{0.5}Co_{0.5}O_3$ is shown in Fig. 9(c). The different particle sizes can be observed for the sample, and some of them were in the range below 100 nm. The images revealed nanostructure of the samples.

Particle diameter of perovskites was determined by dynamic light scattering technique to confirm the existence of nanoparticles through the samples. The results of DLS measurements can be seem in Table 2. The diameter ranges of $LaCoO_3$, $LaMn_{0.25}Co_{0.75}O_3$, and $LaMn_{0.5}Co_{0.5}O_3$ particles are 37-105, 69-159, and 56-241 nm. $LaMn_{0.5}Co_{0.5}O_3$ included larger particles than $LaCoO_3$ and $LaMn_{0.25}Co_{0.75}O_3$. However, the average size of perovskites was less than 100 nm and was in agreement with SEM results.

Catalytic activity of $LaMn_xCo_{1-x}O_3$ perovskites was evaluated in CO+NOx reaction. Results are in Fig. 9. As seen in Fig. 9, by increasing the molar ratio of Mn in $LaMn_xCo_{1-x}O_3$ from 0.1 to 0.25, the catalytic activity was increased. On the other hand, an increase in molar ratio of Mn from 0.25 to 0.5 does not lead to an activity elevation. From selectivity and yield points of view, all the $LaMn_xCo_{1-x}O_3$ perovskites failed in complete converting of NO to N_2 at lower temperatures. By elevation of reaction temperature, N_2O yield decreased and reached zero above 500 °C. Since there was not any significant difference in selectivity of $LaMn_xCo_{1-x}O_3$ perovskites, $LaCo_{0.75}Mn_{0.25}O_3$ could be counted as the optimum formulation for $LaMn_xCo_{1-x}O_3$ perovskites because of its high activity in lower temperatures.

CONCLUSIONS

The catalytic activity of sol gel combustion synthesized $LaB_{0.5}Co_{0.5}O_3$ (B=Cr, Mn, Cu) catalysts was evaluated in CO+NO reaction. Maximum increase in catalytic activity resulted by the partial substitution of Co by Mn. The XRD analysis of catalysts of present survey demonstrated the formation of the claimed perovskite structures. The insertion of Mn into $LaCoO_3$ network in $LaMn_xCo_{1-x}O_3$ catalyst was proven by observing the different main peak 2θ in XRD patterns of mentioned catalysts. Results of BET method, which was utilized to determine the specific surface area of catalysts, did not show significant change of surface area for various perovskite formulations; therefore, the specific surface area of catalysts was not a key parameter for evaluating the of catalytic activity in this study. TPR results showed that $LaMn_{0.5}Co_{0.5}O_3$ has a moderate reduction and oxidation ability at the same time, which is necessary for CO+NO reaction, and this can be assumed the reason of higher activity of $LaMn_{0.5}Co_{0.5}O_3$ in comparison to other $LaB_{0.5}Co_{0.5}O_3$ formulations. Moreover, an optimum value of 0.25 for Mn molar ratio in $LaMn_xCo_{1-x}O_3$ perovskite formulation was revealed by evaluation of catalytic performance of various $LaMn_xCo_{1-x}O_3$ perovskite formulations (x=0, 0.1, 0.25 and 0.5).

REFERENCES

1. F. Ahmed, H. J. Cho, J. K. Kim, N. U. Seong and Y. K. Yeo, *Korean J. Chem. Eng.*, **32**, 1 (2015).
2. A. Fritz and V. Pitchon, *Appl. Catal. B: Environ.*, **13**, 1 (1997).
3. M. D. Amiridis, T. Zhang and R. J. Farrauto, *Appl. Catal. B: Environ.*, **10**, 203 (1996).
4. R. Burch, J. Breen and F. Meunier, *Appl. Catal. B: Environ.*, **39**, 283 (2002).
5. Y. Jia, D. Du, X. Zhang, X. Ding and O. Zhong, *Korean J. Chem. Eng.*, **30**, 1735 (2013).
6. H. Dong, Y. Zhang and Z. Gu, *Korean J. Chem. Eng.*, **31**, 1002 (2014).
7. D. C. Chambers, D. E. Angove and N. W. Cant, *J. Catal.*, **204**, 11 (2001).
8. P. Granger, P. Malfoy, P. Esteves, L. Leclercq and G. Leclercq, *J. Catal.*, **187**, 321 (1999).
9. P. Granger, L. Delannoy, J. Lecomte, C. Dathy, H. Praliaud, L. Leclercq and G. Leclercq, *J. Catal.*, **207**, 202 (2002).
10. P. Bera, K. Patil, V. Jayaram, M. Hegde and G. Subbanna, *J. Mater. Chem.*, **9**, 1801 (1999).
11. N. A. Merino, B. P. Barbero, P. Grange and L. E. Cadús, *J. Catal.*, **231**, 232 (2005).
12. P. Femina and P. Sanjay, *Research Journal of Recent Sciences*, ISSN, 2277, 2502 (2012).
13. M. Alifanti, N. Blangenois, M. Florea and B. Delmon, *Appl. Catal. A: Gen.*, **280**, 255 (2005).
14. T. Screen, *Platinum Metals Review*, **51**, 87 (2007).
15. Y. Nishihata, *Nature*, **418**, 138 (2002).
16. P. Gallagher, D. Johnson and E. Vogel, *J. American Ceramic Soc.*, **60**, 28 (1977).
17. B. Levasseur and S. Kaliaguine, *Appl. Catal. B: Environ.*, **88**, 305 (2009).

18. S. A. Hosseini, M. T. Sadeghi, A. Alemi, A. Niaei, D. Salari and L. Kafi-Ahmadi, *Chinese J. Catal.*, **31**, 747 (2010).
19. J. Kim, T. Kim, J. W. Yoo, K. B. Lee and S.-I. Hong, *Korean J. Chem. Eng.*, **29**, 1329 (2012).
20. A. Giannakas, A. Ladavos and P. Pomonis, *Appl. Catal. B: Environ.*, **49**, 147 (2004).
21. A. Giannakas, A. Leontiou, A. Ladavos and P. Pomonis, *Appl. Catal. A: Gen.*, **309**, 254 (2006).
22. V. Belessi, C. Costa, T. Bakas, T. Anastasiadou, P. Pomonis and A. Efstathiou, *Catal. Today*, **59**, 347 (2000).
23. T. Esaka, H. Sakaguchi and S. Kobayashi, *Solid State Ionics*, **166**, 351 (2004).
24. M. Iwamoto, H. Yahiro, T. Kutsuno, S. Bunyu and S. Kagawa, *Bulletin of the Chem. Soc. Japan*, **62**, 583 (1989).
25. R. Zhang, A. Villanueva, H. Alamdari and S. Kaliaguine, *Appl. Catal. B: Environ.*, **64**, 220 (2006).
26. R. Zhang, A. Villanueva, H. Alamdari and S. Kaliaguine, *Appl. Catal. A: Gen.*, **307**, 85 (2006).
27. H. He, M. Liu, H. Dai, W. Qiu and X. Zi, *Catal. Today*, **126**, 290 (2007).
28. P. Ciambelli, S. Cimino, S. De Rossi, L. Lisi, G. Minelli, P. Porta and G. Russo, *Appl. Catal. B: Environ.*, **29**, 239 (2001).
29. R. Zhang, A. Villanueva, H. Alamdari and S. Kaliaguine, *J. Mol. Catal. A: Chem.*, **258**, 22 (2006).
30. S. A. Hosseini, D. Salari, A. Niaei and S. A. Oskoui, *J. Ind. Eng. Chem.*, **19**, 1903 (2013).
31. J. Zhou, L. Zhao, Q. Huang, R. Zhou and X. Li, *Catal. Lett.*, **127**, 277 (2009).
32. S. Maity, S. Ray and D. Bhattacharya, *J. Phys. Chem. Solids*, **74**, 315 (2013).
33. X. Zhu, Y. Shi, A. Li and Q. Zhong, *Ionics*, **20**, 1011 (2014).
34. J. Dacquin, C. Lancelot, C. Dujardin, P. Da Costa, G. Djega-Mariadassou, P. Beaunier, S. Kaliaguine, S. Vaudreuil, S. Royer and P. Granger, *Appl. Catal. B: Environ.*, **91**, 596 (2009).
35. F. Deganello, G. Marcì and G. Deganello, *J. European Ceramic Soc.*, **29**, 439 (2009).
36. P. Granger, C. Dujardin, J. F. Paul and G. Leclercq, *J. Mol. Catal. A: Chem.*, **228**, 241 (2005).